

Hydraulic Tomography: Continuity and Discontinuity of High- K and Low- K Zones

by David L. Hochstetler¹, Warren Barrash^{2,3}, Carsten Leven⁴, Michael Cardiff⁵, Francesco Chidichimo⁶, and Peter K. Kitanidis²

Abstract

Hydraulic tomography is an emerging field and modeling method that provides a continuous hydraulic conductivity (K) distribution for an investigated region. Characterization approaches that rely on interpolation between one-dimensional (1D) profiles have limited ability to accurately identify high- K channels, juxtapositions of lenses with high K contrast, and breaches in layers or channels between such profiles. However, locating these features is especially important for groundwater flow and transport modeling, and for design and operation of in situ remediation in complex hydrogeologic environments. We use transient hydraulic tomography to estimate 3D K in a volume of 15-m diameter by 20-m saturated thickness in a highly heterogeneous unconfined alluvial (clay to sand-and-gravel) aquifer with a K range of approximately seven orders of magnitude at an active industrial site in Assemini, Sardinia, Italy. A modified Levenberg-Marquardt algorithm was used for geostatistical inversion to deal with the nonlinear nature of the highly heterogeneous system. The imaging results are validated with pumping tests not used in the tomographic inversion. These tests were conducted from three of five clusters of continuous multichannel tubing (CMTs) installed for observation in the tomographic testing. Locations of high- K continuity and discontinuity, juxtaposition of very high- K and very low- K lenses, and low- K "plugs" are evident in regions of the investigated volume where they likely would not have been identified with interpolation from 1D profiles at the positions of the pumping well and five CMT clusters. Quality assessment methods identified a suspect high- K feature between the tested volume and a lateral boundary of the model.

Introduction

A great challenge in understanding and predicting groundwater flow and the movement and fate of substances in the subsurface is accurate estimation of heterogeneity at needed scales of resolution. Complexity of hydrogeology or heterogeneity of hydraulic conductivity (K) has been cited almost universally among main reasons for failure or poor performance of groundwater remediation and monitoring systems (National Research

Council [NRC] 2005, 2013; Illman and Alvarez 2009; Anderson and McCray 2011; Leeson and Stroo 2011; Abriola et al. 2012). Commonly used methods such as slug tests, flowmeter tests, and direct push tests or analysis of borehole samples (e.g., grain size analysis and sample permeameter tests) provide highly resolved estimates, but are one-dimensional (1D) and cannot resolve important details of the continuous, 3D heterogeneous nature of the subsurface (e.g., continuity or discontinuity of high- K and low- K bodies), which are necessary for predicting transport and for remediation method selection, design, and operation (Anderson 1997; Butler 2005; NRC 2005, 2013; Bohling et al. 2007; Castagna and Bellin 2009; Brauchler et al. 2011).

Hydraulic tomography (HT) is a method with potential for providing high-resolution continuous 3D K distributions. 3D transient HT (THT) involves conducting a series of discrete-interval pumping tests with discrete-interval pressure observations at multiple locations, and the data are analyzed through inversion of all tests together. HT has been evolving over the past two decades (Gottlieb and Dietrich 1995); numerical and laboratory examples have contributed to HT operational improvements including increased effectiveness in observation types, times, and networks (e.g., Cardiff et al. 2013b; Sun et al. 2013), and in computational efficiencies (Liu and

¹Corresponding author: Department of Civil and Environmental Engineering, Stanford University, 473 Via Ortega, Room 167A, Stanford, CA 94305; (574) 209-2612; dlhochstetler@gmail.com

²Department of Civil and Environmental Engineering, Stanford University, 473 Via Ortega, Stanford, CA 94305; wbarrash@stanford.edu; peterk@stanford.edu

³Center for Geophysical Investigation of the Subsurface, Department of Geosciences, Boise State University, 1910 University Drive, Boise, ID 83705.

⁴Center for Applied Geoscience, University of Tübingen, Tübingen, Germany; carsten.leven-pfister@uni-tuebingen.de

⁵Department of Geoscience, University of Wisconsin-Madison, Madison, WI; cardiff@wisc.edu

⁶Dipartimento di Ingegneria per l'Ambiente e il Territorio e Ingegneria Chimica, Università della Calabria, via P. Bucci 42B, 87036 Rende, Italy; francescochidichimo@boisestate.edu

Received October 2014, accepted April 2015.

© 2015, National Ground Water Association.

doi: 10.1111/gwat.12344

Kitanidis 2011; Brauchler et al. 2013; Cardiff et al. 2013a; Jiménez et al. 2013; Liu et al. 2013, 2014; Lee and Kitanidis 2014). Cardiff and Barrash (2011) provided a comprehensive summary of 2D and 3D HT studies. To date, there have been more than 20 published field studies using HT, but only a handful (perhaps seven) that provide 3D imaging, and fewer still at the scale of source zones (Kramm et al. 2001) or in situ remediation applications (e.g., surface areas spanning 10s of meters in each direction). Following, we briefly review some of the 3D field THT studies with an emphasis on high-resolution efforts at the source zone or in situ remediation scale.

Brauchler et al. (2010, 2011) used type curve analysis and a travel-time-based tomographic inversion approach with slug interference tests, initially in 2D and then in 3D in a confined sand-and-gravel aquifer at the Stegemuhle research site in Germany. Their method is limited to confined aquifers with K range up to several orders of magnitude, and the modeling approach is computationally efficient. High-resolution diffusivity distribution and K zones with uniform values were imaged in a relatively small investigated volume ($5\text{ m} \times 5\text{ m} \times 2\text{ m}$) with aquifer K range of one order of magnitude.

Berg and Illman (2011a) used 3D THT to estimate K and S_s distributions in a volume of $15\text{ m} \times 15\text{ m} \times 12\text{ m}$ of a highly heterogeneous glaciofluvial confined aquifer-aquitard system at the North Campus Research Site (NCRS) at the University of Waterloo, Canada. They were able to identify the most salient features of the upper part of the system based on comparison to the known geology and to permeameter data where HT observations were also available. Validation results from curve matches with tests not used in the HT inversion were less clear and the authors suggested sources of error may have been too coarse of a numerical grid, and spacing of pumping locations and monitoring ports more than half the correlation length of the aquifer. Cardiff et al. (2012, 2013b) used modular equipment to perform 3D THT in a 20-m diameter by 16.5-m thick volume of an unconfined aquifer at the Boise Hydrogeophysical Research Site (BHRS). Their 3D estimate of K distribution compared well with values of K from slug tests at wells used for HT (Cardiff et al. 2012; Barrash and Cardiff 2013), although the comparison quality was reduced at the top and/or bottom of wells where observation measurements were more sparse or unavailable (see also Liu et al. 2002). In these field demonstrations of 3D THT, Cardiff et al. (2012, 2013b) estimated over 100,000 parameters at high resolution (i.e., values of K at $1\text{ m} \times 1\text{ m} \times 0.6\text{ m}$ voxels) using three points for matching from each of hundreds of drawdown curves. Cardiff et al. (2013b) also quantified the significant reduction in predictive capability of HT for K that occurs when pumping and observation density are reduced.

The main objective of this work is to test the capability of 3D THT to generate high-resolution, accurate 3D K at field scale (e.g., investigated volume about 15 m diameter \times 20 m thickness) in a highly heterogeneous (clay to sand-and-gravel) unconfined sedimentary aquifer

at a hydrologically noisy, contaminated, industrial site with only minimal prior hydrogeological information. In particular, we show that principal features of interest (e.g., continuity and discontinuity of high- K and low- K zones, juxtaposition of high K -contrast bodies) can be imaged with 3D THT where they are not likely recognizable by interpolation between 1D observation locations (wells, continuous multichannel tubing or CMTs [Einarson and Cherry 2002]). We present three methods of evaluation of results that attest to the high quality of the 3D K tomogram overall, while pointing to an area with greater errors and uncertainty where further investigation may be useful. In the process, we show that pumping tests from discrete CMT zones (i.e., tests not included in the inversion) are successfully used for validation, and thus such tests can be low-cost, low-impact, time-efficient supplements or alternatives to conventional pumping tests from discrete zones in wells in unconsolidated sedimentary aquifers. Furthermore, we note additional modeling and field adaptations that supported the high-quality high-resolution imaging of the 3D K distribution for this study.

Field Site and Experimental Design

Brief descriptions of the field site and experimental design for the 3D THT tests of this study are given in the following sections. Additional details on the site, test conditions, equipment, and operational considerations are provided in Supporting Information.

Site Description

The hydrogeological setting for the 3D THT tests of this study is the shallow alluvial aquifer system of the southern Campidano Plains near the Gulf of Cagliari in southern Sardinia, Italy (Ciabatti and Pilia 2004). The HT tests were conducted during a dry period in October 2013 within an industrial site in Assemini where legacy groundwater contamination is captured by on-site treatment by barrier wells at the down-gradient boundary of the site (Figure S1).

The HT testing was conducted within an area of about $20\text{ m} \times 20\text{ m}$ with a specially constructed pumping well (NPM01) and five clusters of CMTs installed with three nested CMTs in each cluster (2×3 -channel and 1×7 -channel) emplaced at 6.7 m to 8.5 m radial distances from NPM01, and at equally spaced radial angles from each other (see Figures 1 and S2). A screened opening of 15-cm length was cut into each CMT channel. Based on site knowledge, 13 openings in each of the CMT clusters were spaced over 15 m from about 19.5 m BLS to the water table ($\sim 5\text{ m}$ BLS) to provide high-density observation coverage for the HT testing (Table S1). Well NPM01 was constructed for this project to support pumping from 15 screened zones, each hydrologically isolated with alternating sand and bentonite in the annular space (e.g., Einarson 2006).

Fiber-optic pressure transducers were used for measuring head changes at observation locations and in the

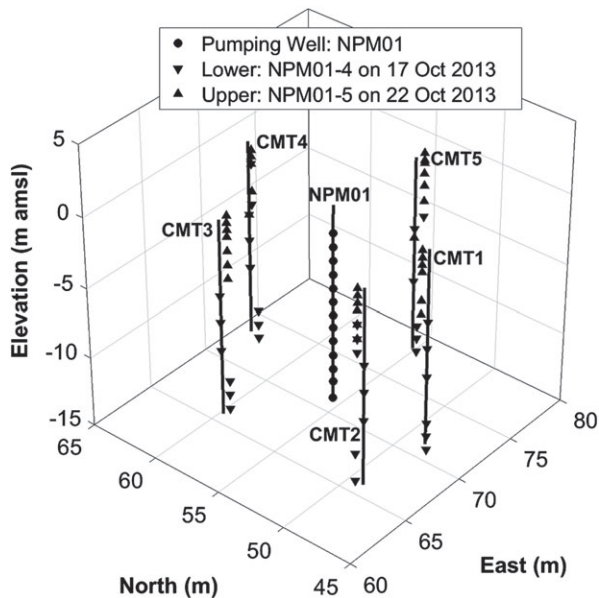


Figure 1. Three-dimensional perspective of pumping intervals (circles) at NPM01 and observation locations (triangles) at CMT locations. Downward pointing triangles are CMT locations used for a test with lower observation zones occupied with transducers (e.g., test using NPM01-4 on 17 Oct 2013) and upward pointing triangles are CMT locations used for a test with transducers in upper observation zones (e.g., test using NPM01-5 on 22 Oct 2013). Coordinates of locations are given in Table S1.

pumping well because of their accuracy and precision (capable of recording head changes ≤ 1 mm), fast and adjustable sampling rate, and small-diameter probe and cable. In particular, the 4 mm transducer diameter allowed insertion into CMTs and into 6.35 mm-diameter tubing used in the straddle-packer pumping system in NPM01 and in the modular, temporary hydraulic packer-and-port system used to limit pressure short-circuiting through a monitoring well (fully screened with sand pack) near NPM01 in the tested volume (Figure S2). For this study, transducers were available to populate only half the observation zones at a time; thus the pumping test series was conducted twice—with observations in lower and upper configurations, respectively (Figure 1, Table 1).

Pumping Tests

Based on previous experience, we anticipated running short-duration pumping tests for the HT campaign (Bar-rash et al. 2006; Cardiff et al. 2012, 2013b). However, given the large range of hydrologic properties associated with the clay to sand-and-gravel aquifer, we conducted pretest modeling to assess pumping rates, pumping times, expected drawdown magnitudes, and necessary recovery times between tests to assure high-quality data with efficient time management. From this analysis, we determined that tests with 15 min of pumping followed by 45 min of recovery would allow the recovery rate to reduce to an insignificant influence on following tests.

A straddle-packer system with a submersible pump between the packers was used for most pumping tests.

In addition, seven pumping tests from CMT zones (using a peristaltic pump) were conducted on a reconnaissance basis; these tests are used for validation of the HT results. Flow rates for all pumping tests were measured using a bucket-and-stopwatch method (e.g., Bohling et al. 2007) due to failure of a digital in-line flowmeter.

Data Analysis and Inversion

In this study, we follow a data analysis approach similar to that developed by Cardiff and Barrash (2011) and Cardiff et al. (2012, 2013b) with modifications to handle the high degree of nonlinearity of this problem. The analysis steps of data selection, forward model development, and inversion are described briefly here; additional detail is given in Supporting Information.

Data Selection

Each pressure transducer records thousands of pressure measurements during the course of a 15-min test. Due to the heterogeneous nature of the volume tested, the range of responses varied greatly; Figure 2 shows examples of differences in response time lag, drawdown magnitude, and curve shape. We found that using four points from each drawdown curve was sufficient to capture diagnostic information (Cooper and Jacob 1946; Boulton 1954; Neuman 1972; McElwee and Yukler 1978) about the unknown parameter field with HT. For efficiency in picking and model setup, we used the same four observation times (i.e., $\sim 10, 40, 150,$ and 860 s) except for tests run for less than 15 min (Table 1). Also note that drawdown magnitudes of ≤ 1 mm are above the noise level of the transducers and provide valuable information (Figures 2 and S5 through S10).

Forward Model

We use MODFLOW (Harbaugh 2005) to simulate the field pumping tests. The top of the modeling domain is the water table. Based on available site reports, we placed a bottom no-flux boundary representing a low-permeability zone approximately 19.5 m below the pretest water table. Given favorable site conditions during the HT testing campaign (noted previously and in Supporting Information), we use constant-head boundary conditions. The overall domain size for all forward models used to simulate pumping tests is $81\text{ m} \times 81\text{ m} \times 9.8\text{ m}$, with the extent of lateral boundaries large enough to limit artificial impacts of constant head boundaries while maintaining a tractable modeling problem. In this regard, we moved boundaries outward when consistent bias was observed in curve mismatches for many tests with only 0.7 mm drawdown influence at boundaries.

The model domain is discretized in cells that are maximum $1\text{ m} \times 1\text{ m} \times 0.6\text{ m}$, with increasing refinement near the pumping well where the smallest cell size is $0.1\text{ m} \times 0.1\text{ m} \times 0.06\text{ m}$. Each MODFLOW model consists of 2.31 million cells. The open well, packers in the well and bentonite rings in the annular space, and gravel rings in the annular space were represented explicitly in the

Table 1**Summary of Pumping Tests from NPM01 (Located at 70.26 m East and 54.86 m North in Local Coordinates)**

Test Date	Pumping Interval	Center of Pump Location (m AMSL)	Average Flow Rate (L/min)	FO Transducer Configuration	Number of FO Transducers Used	Test Duration (min)
16-Oct-2013	1	-13.95	3.49	Lower zones	32	15
17-Oct-2013	2	-12.72	4.60	Lower zones	34	15
17-Oct-2013	3	-11.82	4.80	Lower zones	31	15
17-Oct-2013	4	-10.78	3.00	Lower zones	34	7
17-Oct-2013	5	-9.71	3.20	Lower zones	33	15
18-Oct-2013	6	-8.75	2.05	Lower zones	35	15
18-Oct-2013	7	-7.85	4.05	Lower zones	35	15
18-Oct-2013	8	-6.88	3.42	Lower zones	35	15
18-Oct-2013	9	-5.91	2.88	Lower zones	35	15
18-Oct-2013	10	-4.93	2.49	Lower zones	35	15
18-Oct-2013	11	-3.95	1.74	Lower zones	34	15
18-Oct-2013	12	-2.98	2.62	Lower zones	35	15
21-Oct-2013	13	-1.99	3.29	Lower zones	34	15
21-Oct-2013	15	-0.04	3.33	Lower zones	35	3
21-Oct-2013	1	-13.95	4.99	Upper zones	30	15
22-Oct-2013	2	-12.72	6.97	Upper zones	31	15
22-Oct-2013	3	-11.82	6.35	Upper zones	31	14
22-Oct-2013	4	-10.78	4.41	Upper zones	29	15
22-Oct-2013	5	-9.71	4.49	Upper zones	31	15
22-Oct-2013	6	-8.75	2.51	Upper zones	31	9
22-Oct-2013	7	-7.85	4.17	Upper zones	31	15
22-Oct-2013	8	-6.88	4.44	Upper zones	30	15
22-Oct-2013	9	-5.91	4.31	Upper zones	30	15
23-Oct-2013	10	-4.93	3.53	Upper zones	29	15
23-Oct-2013	11	-3.95	3.50	Upper zones	29	15
23-Oct-2013	12	-2.98	3.79	Upper zones	29	15
23-Oct-2013	13	-1.99	4.13	Upper zones	31	15
23-Oct-2013	14	-1.00	1.90	Upper zones	30	5

model with fixed K values of 1.0 m/s, 4.0×10^{-6} m/s, and 4.0×10^{-3} m/s, respectively. This was necessary to allow MODFLOW to converge for cases where the pumping well was in a low- K zone (see Vesselinov et al. 2001 for another example of explicit treatment of small-scale features in an inversion). Run times for individual MODFLOW simulations on a single core of a conventional desktop PC ranged from less than 2 min to 10 to 20 min. These run-times were largely dependent on the degree of heterogeneity in the parameter field during inversion, and on the rate of pumping and local rates of drawdown for a given test.

Inversion

For tomographic imaging of the aquifer properties, we use the Bayesian-based geostatistical inversion approach of Kitanidis and Vomvoris (1983) and Kitanidis (1995), with modifications for solving the optimization problem. Here we briefly summarize our implementation and modifications; more complete descriptions of using the geostatistical approach for inversion of HT data are given in Supporting Information and in Cardiff and Barrash (2011) and Cardiff et al. (2012, 2013b). The relationship between the data and the unknown parameter field is through the forward model. We assume the error in this relationship, due to both measurement noise and

an imperfect model, to be normally distributed with zero mean and to be independent. The parameter field is assumed to be stationary with a mean that can be expressed by the product of known drift functions and unknown drift coefficients and by a covariance function. From the drawdown data, 3336 data points were used to invert for 2.17×10^5 unknown parameters (Table 2). The unknown parameter field was uniformly discretized into $1 \text{ m} \times 1 \text{ m} \times 0.6 \text{ m}$ cells, which encompassed single or multiple MODFLOW grid cells if the location was away from or near the center of the model domain, respectively. We use the adjoint MODFLOW solver of Clemo (2007) to compute the sensitivity matrix of observations to unknowns, where the time to do so equals the time to solve MODFLOW simulations for the number of observations plus one. The objective function to be optimized balances data fitting and plausibility of the estimated parameter field.

Previous implementation of the quasi-linear geostatistical approach has included a line search between the current and new parameter fields in order to ensure reduction in the objective function at each iteration (Cardiff et al. 2012, 2013b). Due to the highly heterogeneous nature of the site, we used the modified Levenberg-Marquardt (L-M) approach to the geostatistical method (Nowak and Cirpka 2004). The L-M approach is a hybrid of the

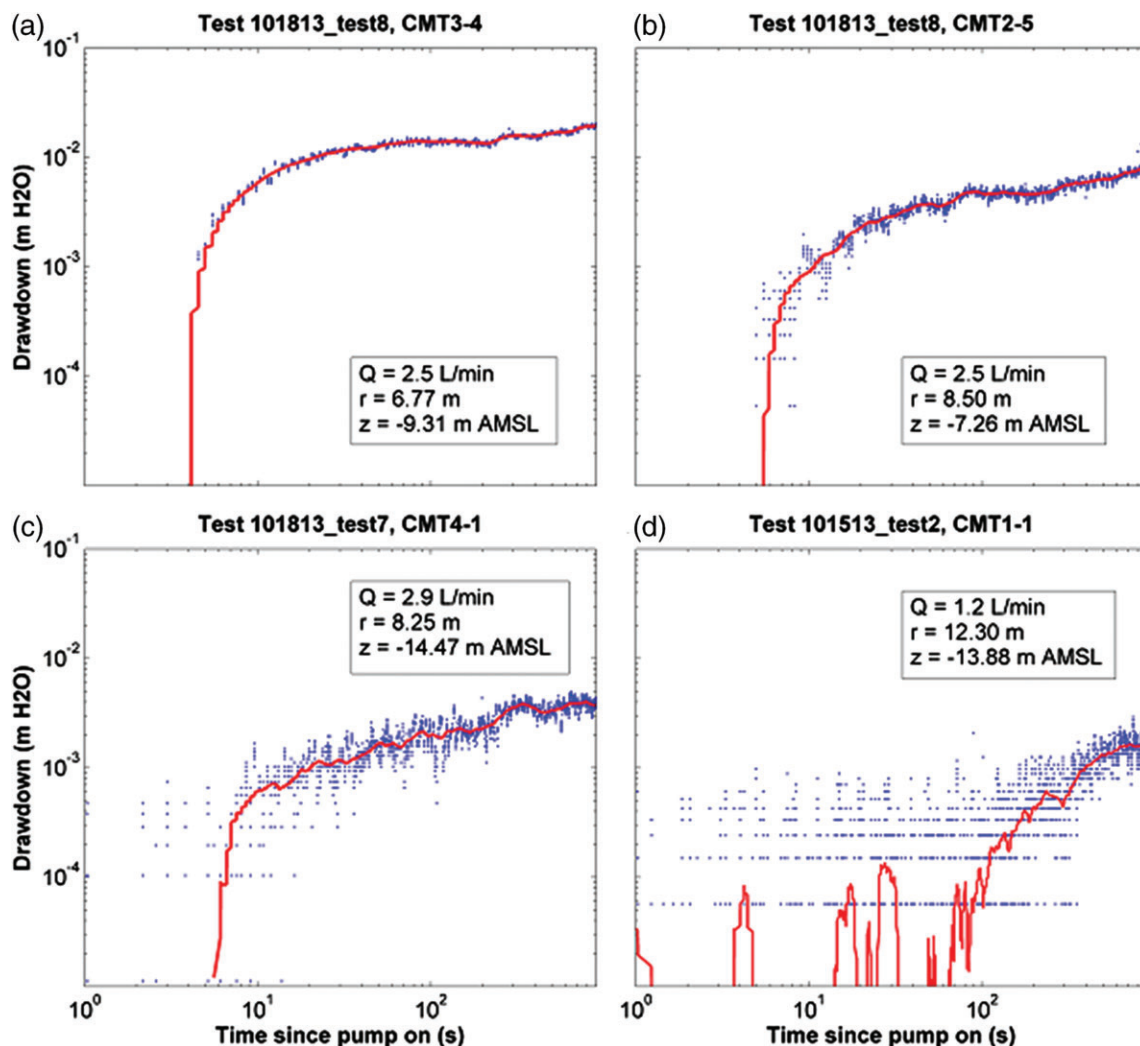


Figure 2. Example drawdown curves illustrating the range of responses in magnitude, time lag to drawdown initiation, and curve shape. Q is pumping rate, r is lateral distance from a pumping zone to an observation location, and z is the vertical coordinate of an observation location. Red lines are moving averages of drawdown measurements. Results shown for: (a) pumping interval NPM01-10, observations at CMT3-4, (b) pumping interval NPM01-10, observations at CMT2-5, (c) pumping interval NPM01-9, observations at CMT4-1, and (d) pumping interval CMT3-2, observations at CMT1-1.

Table 2
Size of the 3D THT Problem at an Active Industrial Site

Pumping Tests Used	Draw-down Curves	Observation (Data) Points Used (n)	Cells in Each MODFLOW Model	Parameters Inverted (m)
26	834	3336	2.31×10^6	2.17×10^5

Gauss-Newton and steepest-descent methods that works well for problems that are more strongly nonlinear (Pujol 2007). Finally, within this Bayesian framework, we can estimate the uncertainty of the K field, represented as the normalized standard deviation, by using the square root of the diagonal of the posterior covariance matrix (see Supporting Information).

In this study, we are interested in imaging the 3D heterogeneous K field, but we also solve for constant values of the storage parameters S_s and S_y . Cardiff and Barrash (2011) demonstrated that using reasonable constant values for S_s and S_y does not significantly impact estimates of the heterogeneous K field.

Tomographic Imaging Results

The goal is to estimate the K field at this site with resolution of sufficient detail for potential source zone remediation. The 3D THT imaging results identify many hydrogeological features with a range of K across almost seven orders of magnitude and geometric mean value of the best estimate of the K field equal to 1.3×10^{-5} m/s (Figures 3 and 4). The constant values of “effective” S_s and S_y for the site are estimated by the inversion to be $2.8 \times 10^{-5} \text{ m}^{-1}$ and 6.6×10^{-3} , respectively. Small values for S_y in short-duration pumping tests are well

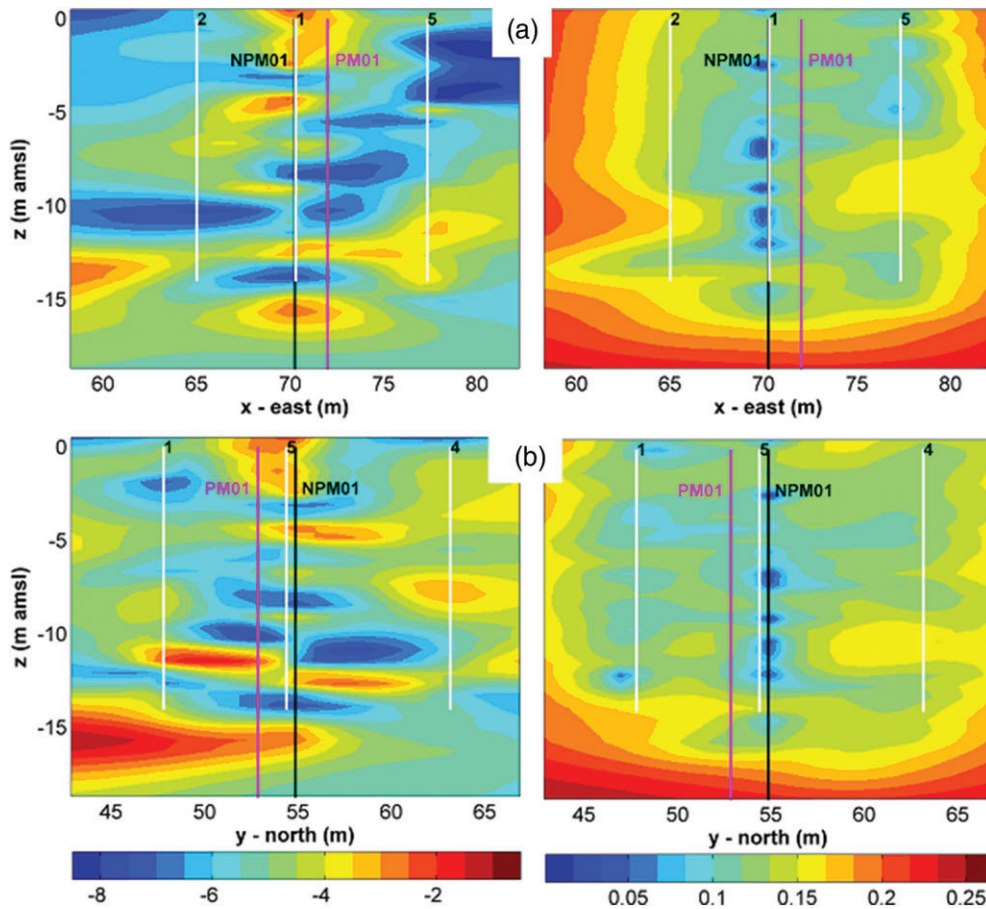


Figure 3. Two-dimensional vertical transects of the estimated $\log_{10}(K$ [m/s]) field (left) and the corresponding uncertainty or posterior standard deviation normalized by the range of the $\log_{10}(K$ [m/s]) (right). The top images are in the easting direction ($y = 54.9$ m) (a), while the bottom images are in the northing direction ($x = 70.3$ m) (b). Both images are centered at the pumping well NPM01. CMTs are shown for perspective on lateral distances and are not necessarily in these exact planes.

documented (Walton 1970, table 4.9; Neuman 1975; Moench 1994; Chen and Ayers 1998; Barrash et al. 2006). Two perpendicular cross-sections centered at NPM01 in Figure 3 show the high variability in K at the site (panels on the left) as well as the relative uncertainty in the estimation (panels on the right). The imaging results show multiple layers or lenses of both low K (i.e., silty-clayey materials with $K < 10^{-6}$ m/s) and high K (i.e., sand-and-gravel material with $K > 10^{-3}$ m/s) including abrupt juxtapositions of high K -contrast lenses.

The ability of HT to capture detailed hydrogeologic features in 3D such as continuity and discontinuity of high- K and low- K zones, is illustrated in Figure 4. The three rows of Figure 4 give orthogonal vertical planes of the best estimate of the $\log_{10}K$ field, and the same slices of the relative uncertainty, at three orientation perspectives. Example hydrogeologic features identified in Figure 4 that are important for flow and transport are: a low- K “plug”; a sloping high- K zone of continuity between two higher K lenses; a discontinuity between two higher K lenses at approximately the same elevation; and very low- K and very high- K lenses in close vertical proximity (i.e., minimal smoothing). All of these significant features (except perhaps the low- K plug) would be difficult or

impossible to identify with interpolation from 1D profiles at similar positions.

Quality of Results

We assess the quality of the tomographic solution for the 3D K distribution with three methods that have been used previously for 3D THT (Berg and Illman 2011a, 2011b; Cardiff et al. 2012, 2013b; Illman 2014): (1) quality of calibration, or goodness of matches between observed drawdown curves from HT pumping tests used in the tomography and simulated drawdown curves; (2) distribution of uncertainty calculated for the tomographic results; and (3) quality of validation, or goodness of matches between observed drawdown curves and curves from simulated pumping tests at CMTs (i.e., tests not used in the tomography and at locations not close to the pumping well used for tomography). For both sets of comparison scenarios (i.e., (1) and (3) above), the estimated K distribution from the HT results is used for simulations. Although it is common also to compare HT results locally with independent 1D profiles at wells, DP, or CMT locations, such independent data are not available at the Assemini site investigated for this study.

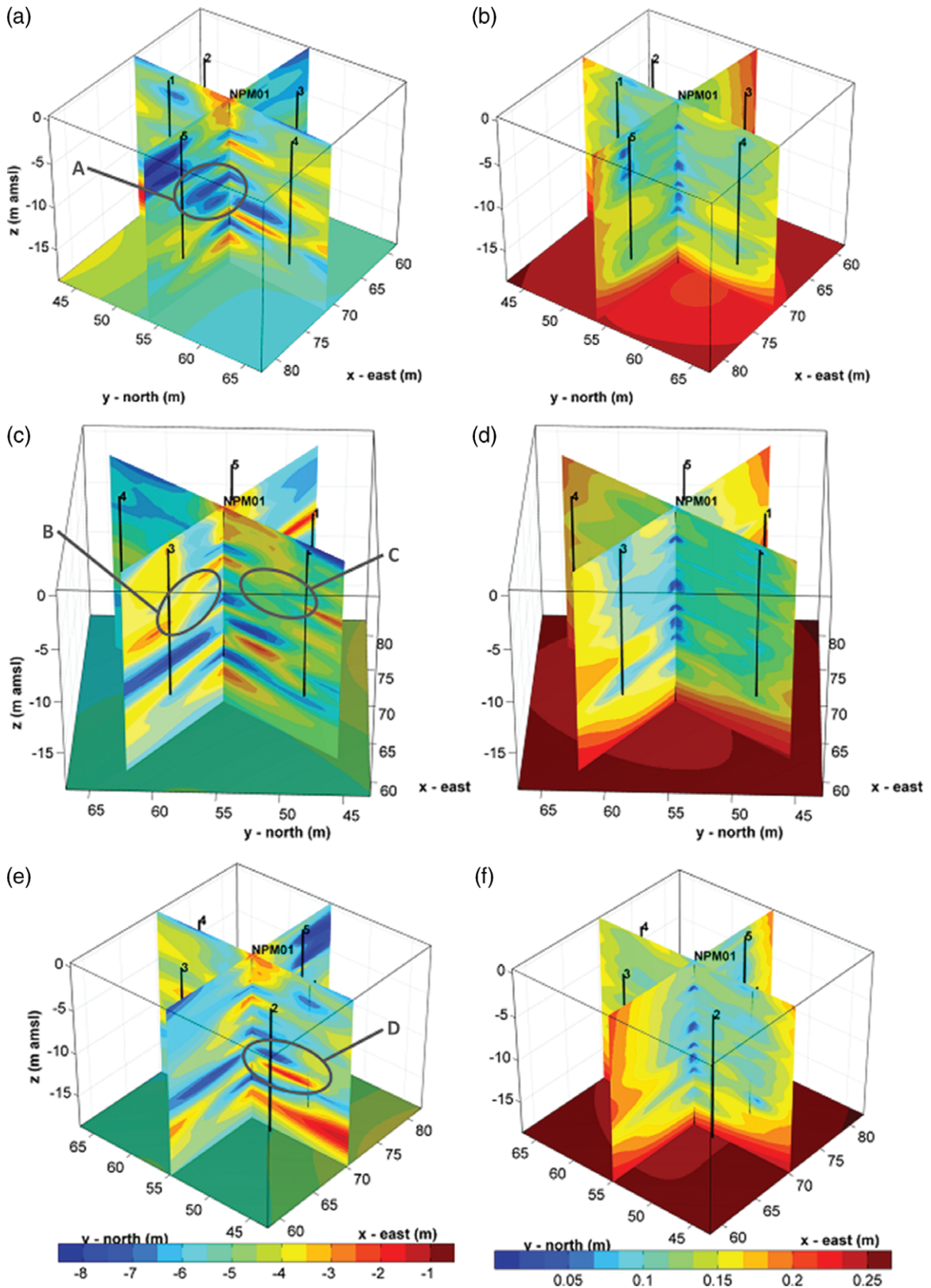


Figure 4. Slices intersecting at NPM01 illustrate the estimated $\log_{10}(K \text{ [m/s]})$ field (left: a, c, e) and corresponding uncertainty or posterior standard deviation normalized by the range of the $\log_{10}(K \text{ [m/s]})$ (right: b, d, f) from three perspectives through the tomographic volume of interest, primarily between NPM01 and CMTs. Important hydrogeologic features identified in outlined zones A to D are: A in (a), a low- K “plug”; B in (c), a sloping high- K zone of continuity between two higher- K lenses; C in (c), a discontinuity between two higher- K lenses at approximately the same elevation; D in (e), vertically adjacent very low- K and very high- K lenses in close proximity (i.e., minimal smoothing).

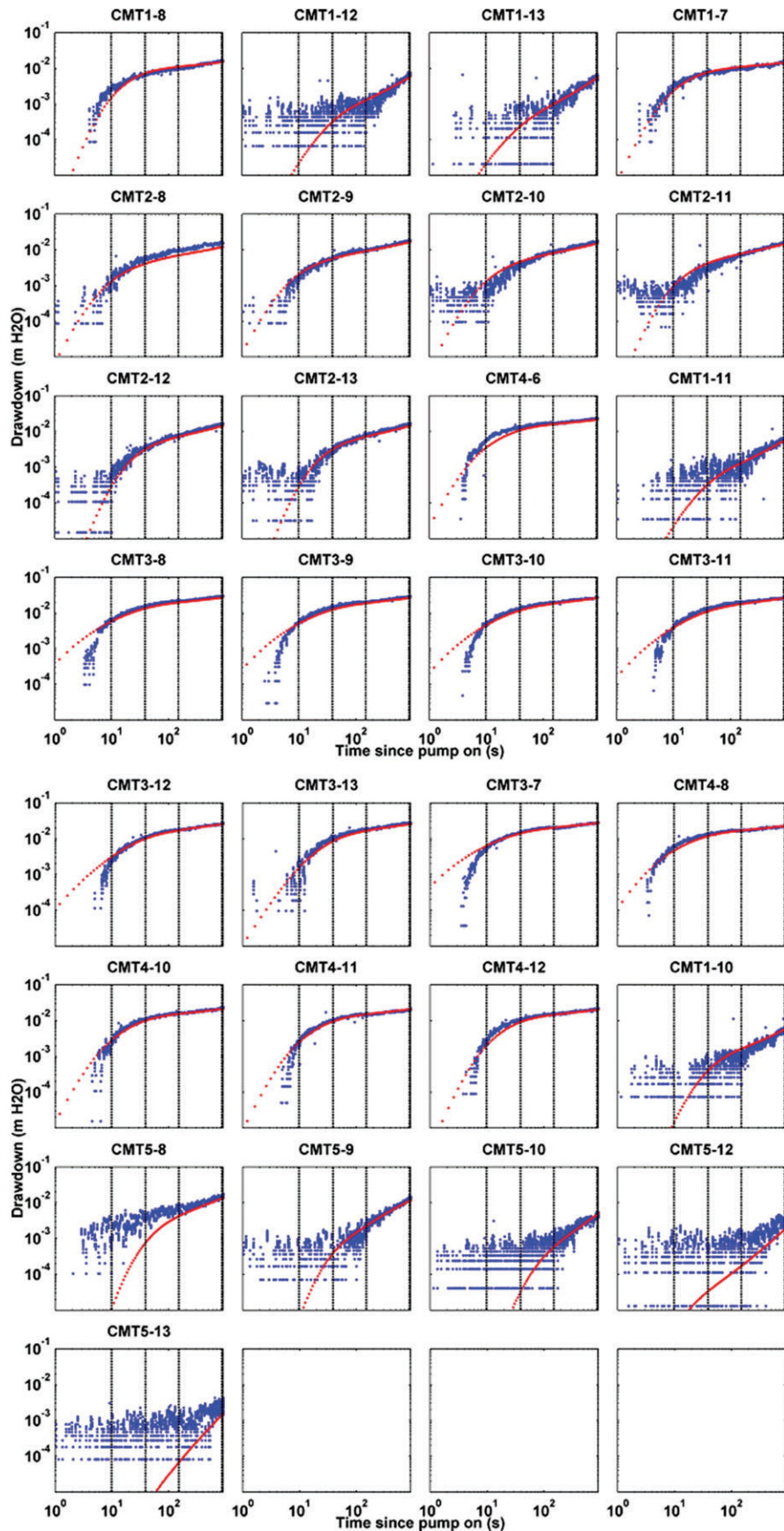


Figure 5. Model calibration or simulation matches to drawdown curves from test NPM01-10. Blue dots are measurements from the field, red dots are simulated observations using the best estimated parameter field from the inversion, and black dashed lines indicate times at which measurements were used for data matching in the inversion.

Model Calibration or Curve Matching of HT Tests

The inversion results are based largely on measurements from the field HT testing while also accounting for the general prior information used. Thus, with consideration of errors in measurements and models, we expect that the forward model with the best estimate of the parameter field will be able to closely reproduce the observations. For example, Figure 5 shows close matches between observed drawdown curves of pumping test NPM01-10 with corresponding drawdown curves simulated by the forward model using the best estimate K distribution from the tomographic inversion.

Figure 6 shows a crossplot of the 3336 measured vs. simulated data points for all 26 tests used in the tomographic inversion. Overall, forward simulations using the estimated K field and values for S_s , and S_y reproduce the field data quite well, as quantified by a regression slope of 0.9 and $r^2 = 0.94$. However, there is a slight trend of under prediction (10%) for larger drawdowns. A plausible reason for this bias of reduced observed drawdown is some release of water from the constant head lateral boundaries when pumping effects reach the boundaries at later times in a given test.

Uncertainty Calculations for the Imaging Results

Although the true K field is unknown, we can quantify the relative confidence we have in the imaging results by calculating the K field uncertainty as the posterior standard deviation of the K field normalized by the range of values of the estimated field (see Supporting Information and Cardiff et al. 2012, 2013b). This is a metric for relative confidence in estimated K at a given location. As expected given the close matches to calibration curves, confidence in the estimates is high (with few exceptions) in the volume bounded by the observation locations (CMTs). Uncertainty in K estimates increases below -14 m AMSL, likely due to reduced observation density below a certain depth and uncertainty in the bottom boundary condition of the model.

Validation with CMT Pumping Tests Not Used in the HT Inversion

The typical goal in parameter estimation is to have much improved predictive capability. For this research,

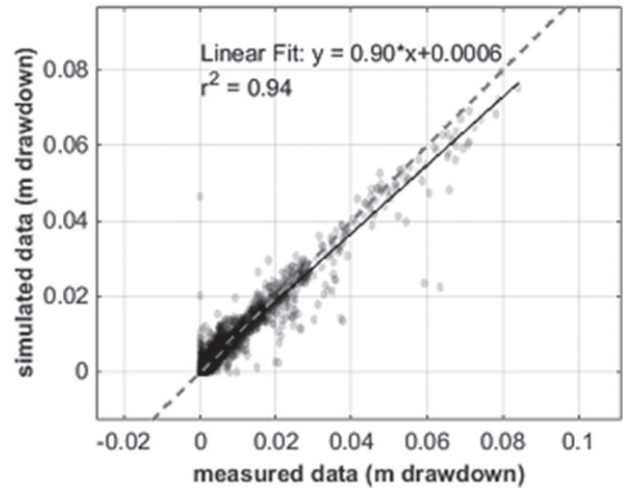


Figure 6. Crossplot of measured vs. simulated drawdown at each of the 3336 match points from the 26 tests used in the tomographic inversion. Linear regression line in black with corresponding regression equation and r^2 , and 1:1 line (dashed) for reference.

we desire quantitative K estimates at sufficient resolution to support accurate predictions of flow and transport in the context of remediation. In this regard, perhaps the best form of validation is to test whether a model with the estimated parameter field can predict the system response under different conditions than were used for data collection and tomographic parameter estimation (Liu et al. 2007; Berg and Illman 2011a, 2011b; Cardiff et al. 2013b; Illman 2014). We tested the ability of our estimated parameter field (i.e., 3D THT results presented above) to reproduce the drawdowns from seven additional pumping tests not used in the tomographic inversion. These tests involved pumping at three of the five CMT clusters at the perimeter of the tested volume (Figures 1 and S2). A peristaltic pump was used to pump at lower rates (Table 3) from the small diameter, small open-interval CMT ports. Figure 7 shows drawdown match comparisons for the validation pumping test at CMT3-7. Plots of drawdown comparisons for the remaining six validation tests are provided in Figures S5 to S10 for completeness. Additionally, Figure 8 summarizes

Table 3
Pumping Tests from CMTs Used for Inversion Validation

Test Name	Pumping Well	Pumping Interval	Center of Pump Location (m AMSL)	FO Transducer Configuration	Average Flow Rate (L/min)	Test Duration (min)
15 Oct 2013 Test 1	CMT3	7	-4.12	Lower zones	1.3	15
15 Oct 2013 Test 2	CMT3	2	-12.89	Lower zones	1.2	15
28 Oct 2013 Test 10	CMT3	4	-9.31	Lower zones	1.5	15
28 Oct 2013 Test 11	CMT1	2	-12.88	Lower zones	1.5	15
29 Oct 2013 Test 1	CMT1	7	-4.33	Lower zones	1.4	15
29 Oct 2013 Test 2	CMT1	4	-9.06	Lower zones	1.5	15
29 Oct 2013 Test 3	CMT5	2	-13.58	Lower zones	1.6	15

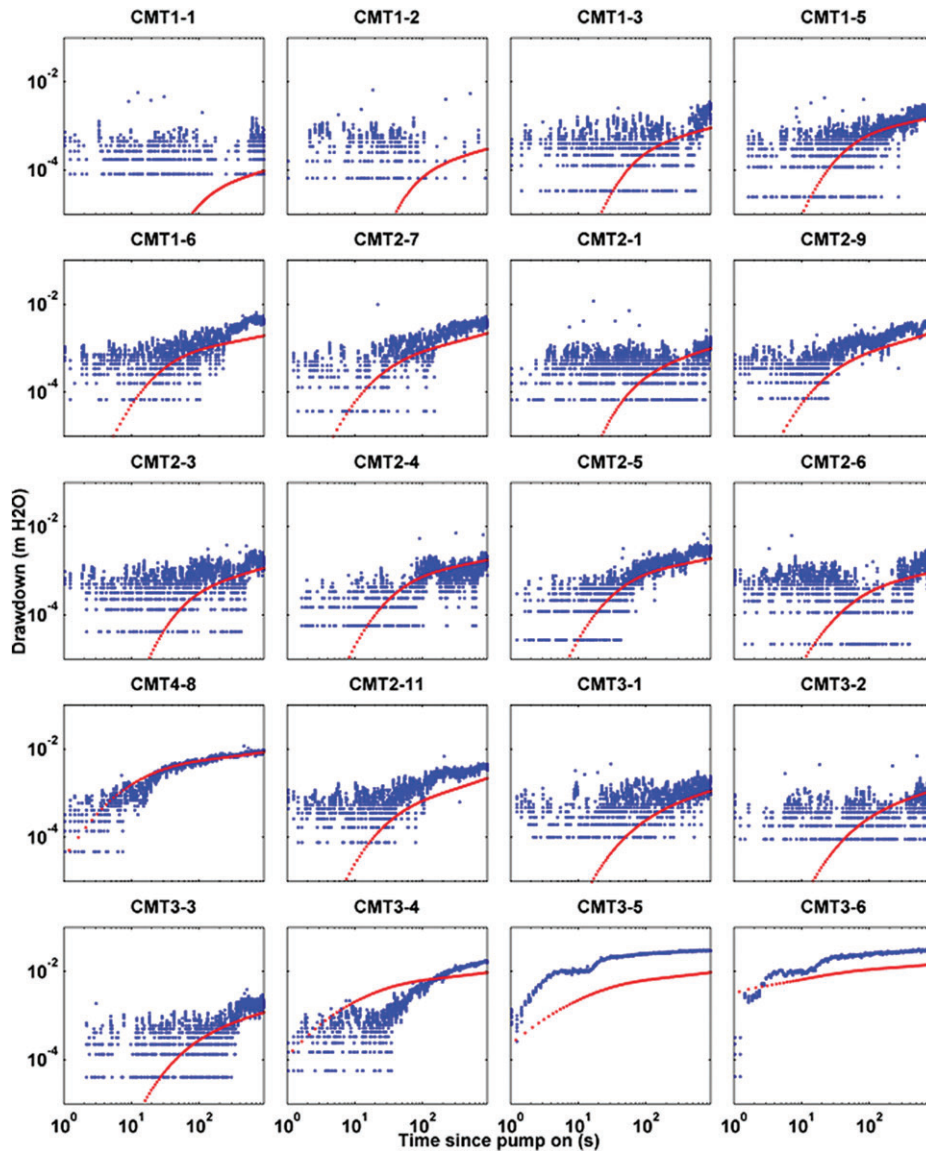


Figure 7. Drawdown observations from field validation test with pumping from CMT 3-7 (blue), and corresponding predicted drawdowns using forward model with best estimated parameter field from inversion (red).

validation test results with crossplots of measured vs. simulated drawdown.

Results of the validation test at CMT3-7 (Figure 7) are representative of five of the seven validation tests (CMT1-7, CMT3-2, CMT3-4, CMT3-7, and CMT5-2). Common observations across these five tests are:

1. At most observation locations, the model using the estimated K field, S_s , and S_y closely predicted drawdowns from the validation tests.
2. At observation locations vertically close to the pumping location in a given CMT cluster, the model did not accurately predict measured responses (see drawdown curves at CMT3-4, CMT3-5, and CMT3-6 in Figures 7 and S5 to S10). For example, drawdown is under predicted at: CMT3-3 with pumping at CMT3-2; CMT1-3 with pumping at CMT1-2; CMT1-6 with pumping at CMT1-7.

With respect to the second point above: because the anomalously high drawdowns are only observed in zones that are vertically near a given pumping zone (Figures 7 and S5 to S10), it appears likely that incomplete collapse and/or incomplete sand fill in the annular space between the CMTs and the borehole wall allows vertical communication with vertically nearby pumping zones.

Two validation tests (pumping at CMT1-2 and CMT1-4) have anomalous results compared with the other five tests; they consistently under predict observed drawdowns at (1) nearly all observation locations for pumping at CMT1-2, and (2) at numerous locations for pumping at CMT1-4 (but with less-severe under prediction than for pumping at CMT1-2; e.g., compare Figure 7 with Figures S7 and S9). A plausible reason for the discrepancies of pumping tests at CMT1-2 and CMT1-4 is the high- K lens below CMT1-2 (see Figure 3b [left panel] and Figure 4e near $x = 70$ m, $y = 45$ m) which is

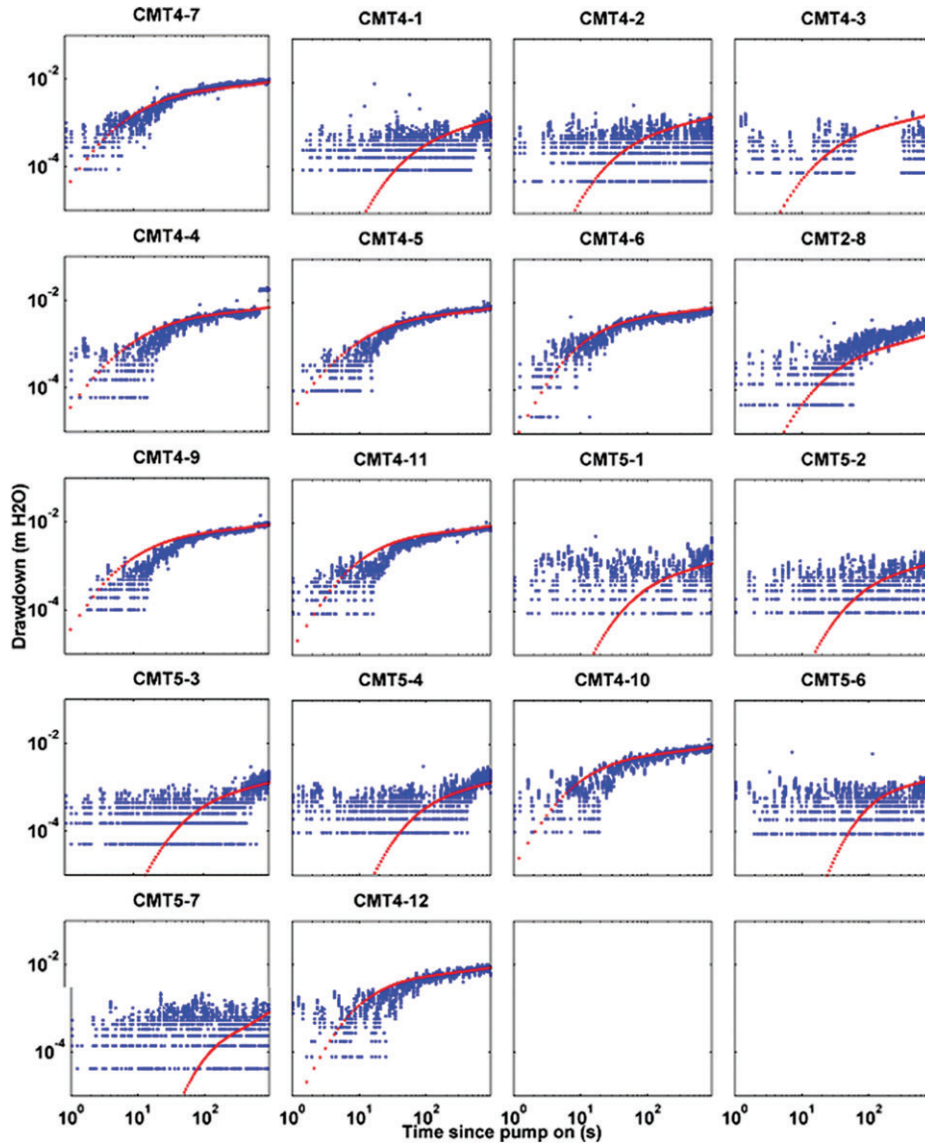


Figure 7. Continued

a suspect feature. Indeed, this high- K lens occurs in the local area of higher uncertainty at the bottom of the tested volume (Figure 3b) and can be traced as a very high- K channel outside the tested volume to the lateral constant-head boundary of the model.

Such a high- K feature adjacent to CMT1-2 that connects to a constant-head source of water can explain suppressed simulated drawdown during a pumping test in the tested volume, and is consistent with the pattern of improved curve matching with pumping tests progressively further (vertically) away from the high- K feature (i.e., less-severe mismatches for the pumping test at CMT1-4 vs. CMT1-2, and minimal issues for the pumping test at CMT1-7 [Figure S8]). Indeed, confidence in the robustness of the quality-evaluation measures of uncertainty quantification and validation tests is gained because both have identified the same region of the 3D tomography image that is not well reproduced. In this regard, one working hypothesis consistent with available information

is: the high- K connection to the constant-head boundary (which is, without other context, a rather prominent structure to occur in the data-starved region between the CMTs and the model lateral boundary) appears to be a model-error compensation for a model-error assumption of no-flow at the bottom boundary, at least locally below CMT-1. This region then could be (1) a target for follow-up investigation or (2) considered with caution where such follow-up is not possible.

Comparison with Published Field and Laboratory Validation Results

Overall, these validation results are very encouraging and provide credibility to the tomographic inversion. Indeed, crossplots of observed vs. predicted or simulated drawdown for the CMT validation tests (especially those minimally affected by the suspect or uncertain high- K body near CMT1) show close adherence to the 1:1 line and mostly high r^2 values (Figure 8, Table 4). For perspective

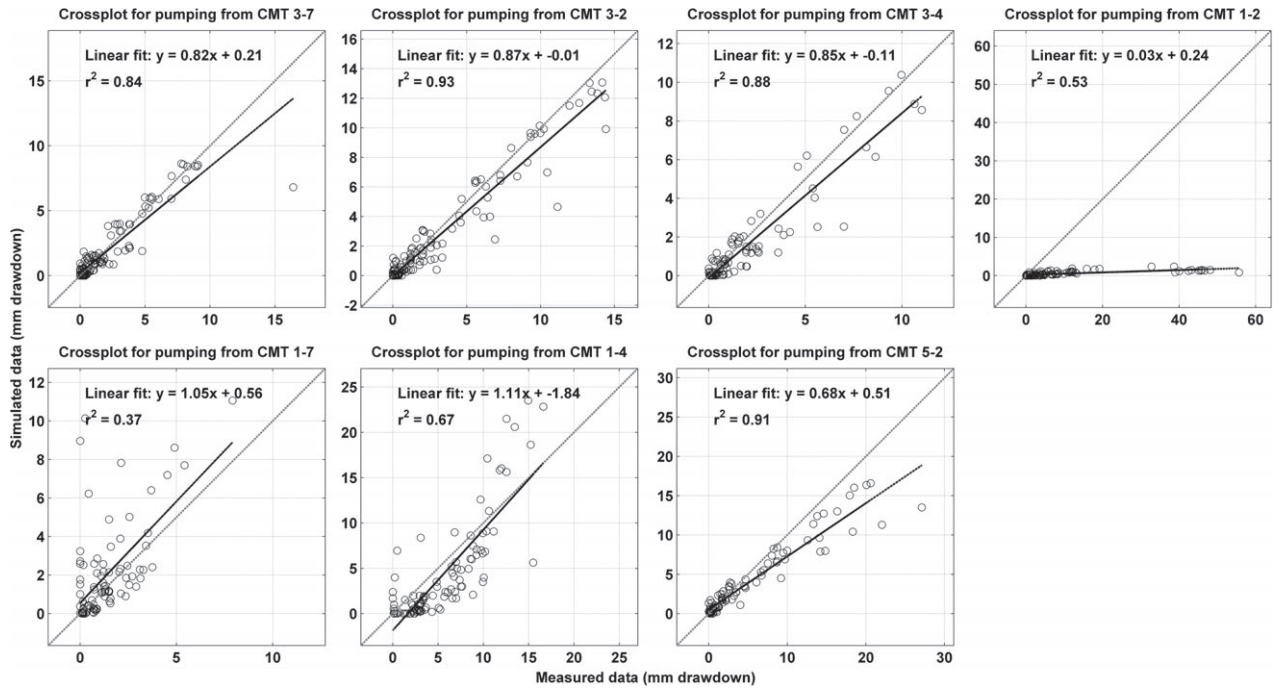


Figure 8. Crossplots of measured vs. simulated drawdown points for additional pumping tests used for validation, along with: linear regression lines (in black); regression equations; and r^2 values. 1:1 lines (dashed grey) for reference. Drawdown results for observation zones vertically adjacent to pumping ports are excluded due to suspected incomplete collapse during CMT installations. Note varying scales between crossplots.

Table 4
Comparison of Validation Test Results for 3D THT of This Study with Validation Tests of 3D THT at the NCRS (Berg and Illman 2011a, Figure 13¹) and Laboratory THT (Berg and Illman 2011b)

							Average
<i>The present study</i>							
Test	CMT1-4	CMT1-7	CMT3-2	CMT3-4	CMT3-7	CMT5-2	$n = 6^2$
Slope	1.11	1.05	0.87	0.85	0.82	0.68	0.16^3
r^2	0.67	0.37	0.93	0.88	0.84	0.91	0.77
<i>NCRS</i>							
Test	PW1-4	PW1-5	PW-3-4	PW5-4	PW5-5	—	$n = 5^1$
Slope	0.14	0.70	0.34	0.32	0.32	—	0.64^3
r^2	0.12	0.56	0.28	0.15	0.24	—	0.27
<i>Laboratory</i>							
Test	Port 18	Port 23	Port 40	Port 42	—	—	$n = 4$
Slope	1.03	1.04	1.03	1.21	—	—	0.08^3
r^2	0.95	0.90	0.98	0.98	—	—	0.95

¹Note we only use validation tests in this table (i.e., tests that were not included in HT inversion); calibration tests in Figure 13 of Berg and Illman (2011a) that were used in HT inversion are not included here for comparison.

²Six of seven validation tests are used from this study; the test with pumping from CMT1-2 is not used because of the dominant influence on this test of leakage through a suspect high- K connection to a lateral boundary (Figures 8 and S7).

³Average slope values are given as average absolute value differences from the 1:1 line, or $(|1.0 - \text{slope}|)$ and a perfect match would yield 0.00.

on quality, we compare these validation results (Figure 8) with validation using the same method for (1) field 3D THT in a largely similar but confined clay to sand-and-gravel aquifer (Figure 13 in the study by Berg and Illman 2011a) and (2) laboratory THT in a less-heterogeneous sandy aquifer (Figure 8 in the study by Berg and Illman 2011b). Quantitative validation results from this study (i.e., curve-match slope and r^2 values) are much closer to laboratory quality than previous field 3D THT in a

comparably heterogeneous aquifer setting (Table 4). Here we note that Berg and Illman (2011a) conducted one of the first 3D THT field studies, which was more a proof-of-concept study than a detailed high-resolution study.

Summary and Conclusions

3D THT can generate high-resolution tomograms in highly heterogeneous unconfined aquifers (e.g., clay to

sand-and-gravel aquifers with almost seven orders of magnitude K range) that can identify hydrogeological features (e.g., continuity and discontinuity of high- K and low- K zones, juxtaposition of high- K and low- K lenses) that would not be identified by interpolation of 1D information between wells. Such features are important for accurate flow and transport modeling and for selection, design, and operation of remediation systems.

Modeling of the unconfined, highly heterogeneous aquifer at high resolution was accomplished using MODFLOW with the adjoint state method for calculating the sensitivity matrix and a modified Levenberg-Marquardt solver for the nonlinear geostatistical inverse problem. The forward models were highly discretized to account for high K contrasts and infrastructure at the pumping well. The unknown parameter field was uniformly discretized into $1\text{ m} \times 1\text{ m} \times 0.6\text{ m}$ voxels to provide high-resolution of heterogeneity.

High-resolution tomograms generated by 3D THT in the field are evaluated by uncertainty quantification, match quality and match-point statistics of calibration curves, and match quality and match-point statistics of validation curves. Evaluation results approach laboratory quality for most of the tomogram within the perimeter of observation CMTs. Higher uncertainties and poorer validation matches and match statistics are associated with the location below and to the side of CMT1 where a suspect feature is identified and thereby provides valuable information for follow-up investigation or caution in interpretation.

Taken together, results and evaluation of results from this study indicate that high-resolution 3D THT can be conducted successfully at hydrologically noisy, active industrial sites if care is taken to plan for appropriate site infrastructure (in this case, installation of a pumping well with alternating sand and bentonite, and nested CMTs), monitor for trends, mitigate open-well influences, and operate timing of pumping tests and recovery to maximize the number of tests while minimizing recovery-trend effects and the volume of contaminated water to be captured.

A key enabling technology contributing to the high quality of the tomogram is high-resolution ($\leq 1\text{ mm}$ head change), fast-sampling, small-diameter, fiber-optic pressure transducers that allow efficient access to observation zones through small-diameter tubes. Also, the new and easily transferable testing capability of pumping from CMT zones was demonstrated and provided strong validation test evidence for this study.

Acknowledgments

We gratefully acknowledge the support of Eni S.p.A. under research contract 4310049886 with Stanford University. We thank Luciano Zaninetta, Giorgio Bianchi, Riccardo Mercuri, Antonio Pisu, and others for their planning, logistical, and administrative support; Riccardo Borella for his support in the field; and Murray Einarson for his discussion on well construction. Also, we thank Geoff Bohling and two anonymous reviewers

for constructive comments which helped improve this article.

Supporting Information

Additional Supporting Information may be found in the online version of this article:

Appendix S1. Supporting details of hydraulic tomography testing in Sardinia.

Appendix S2. Supporting details of forward and inverse modeling.

Table S1. CMT observation locations.

Figure S1. Aerial view of industrial site with groundwater flow direction indicated by arrows. Inset shows the area surrounding HT testing and footprint of HT testing area (gray square—also see Figure S2). Black circles indicate barrier pumping wells and red circles identify monitoring wells that had data loggers recording water levels prior to and during the HT testing campaign. Note that pumping from barrier well PR01 was turned off seven days prior to, and for the duration of, HT testing.

Figure S2. Overview of the testing area with identified features including: new pumping well (NPM01), pre-existing monitoring well (PM01), observation locations (CMTs), and relevant data collection systems.

Figure S3. Hydrographs from three monitoring wells spanning the period of HT tests: SB41 (top), P6 (middle), and PC032 (bottom). SB41 is nearest to the HT testing site, while P6 and PC032 are further away, up gradient and down gradient, respectively (see Figure S1). Water levels are all relative to the level measured at 00:00 on October 11, 2013 for ease of comparison. The approximate periods during which HT pumping tests occurred on a given day are shown as shaded intervals for pumping tests from NPM01 (in aqua), the CMTs (in lime green), and PM01 (in gray). Note that the testing from PM01 was not described or used in this paper; those testing dates are shown for completeness. This figure shows daily cycles (two per day), several 5- to 7-day cycles, and a superimposed regional-scale downward trend.

Figure S4. Hydrographs focusing on the daily trends in three monitoring wells: SB41, P6, and PC032. Water levels are all relative to the level measured at 00:00 on October 23, 2013 for ease of comparison. All monitoring wells show twice-daily fluctuations on the order of 0.01 m over 6 h for a rate of approximately $5 \times 10^{-7}\text{ m/s}$, which yields a water level change of $\ll 0.001\text{ m}$ during a 15-min period (i.e., the length of a pumping test).

Figure S5. Drawdown observations from field validation pumping test from CMT3-2 on October 15, 2013 (blue), and the corresponding predicted drawdown using forward model with best estimated parameter field from inversion (red).

Figure S6. Drawdown observations from field validation pumping test from CMT3-4 on October 28, 2013 (blue), and the corresponding predicted drawdown using forward model with best estimated parameter field from inversion (red).

Figure S7. Drawdown observations from field validation pumping test from CMT1-2 on October 28, 2013 (blue), and the corresponding predicted drawdown using forward model with best estimated parameter field from inversion (red).

Figure S8. Drawdown observations from field validation pumping test from CMT1-7 on October 29, 2013 (blue), and the corresponding predicted drawdown using forward model with best estimated parameter field from inversion (red).

Figure S9. Drawdown observations from field validation pumping test from CMT1-4 on October 29, 2013 (blue), and the corresponding predicted drawdown using forward model with best estimated parameter field from inversion (red).

Figure S10. Drawdown observations from field validation pumping test from CMT5-2 on October 29, 2013 (blue), and the corresponding predicted drawdown using forward model with best estimated parameter field from inversion (red).

References

- Abriola, L.M., J.A. Christ, K.D. Pennell, and C.A. Ramsburg. 2012. Chapter 10: Source remediation challenges. In *Delivery and Mixing in the Subsurface: Processes and Design Principles for In Situ Remediation*, ed. P.K. Kitanidis and P.L. McCarty, 239–276. New York: Springer.
- Anderson, M.P. 1997. Characterization of geological heterogeneity. In *Subsurface Flow and Transport: A Stochastic Approach*. UNESCO International Hydrology Series, ed. G. Dagan and S.P. Neuman, 23–43. New York: Cambridge University Press.
- Anderson, M.P., and J. McCray. 2011. Foreword: Lessons learned about contaminant hydrogeology from legacy research sites. *Ground Water* 49, no. 5: 617–619.
- Barrash, W., and M. Cardiff. 2013. Hydraulic conductivity distribution from multi-level slug tests and multivariate facies associations in a conglomeratic fluvial aquifer, Boise Hydrogeophysical Research Site. BSU CGISS Technical Report 13-03. Boise, Idaho: Boise State University.
- Barrash, W., T. Clemo, J.J. Fox, and T.C. Johnson. 2006. Field, laboratory, and modeling investigation of the skin effect at wells with slotted casing. *Journal of Hydrology* 326, no. 1-4: 181–198. DOI:10.1016/j.jhydrol.2005.10.029.
- Berg, S.J., and W.A. Illman. 2011a. Three-dimensional transient hydraulic tomography in a highly heterogeneous glaciofluvial aquifer-aquitard system. *Water Resources Research* 47, no. 10: W10507. DOI:10.1029/2011WR01016.
- Berg, S.J., and W.A. Illman. 2011b. Capturing aquifer heterogeneity: Comparison of approaches through controlled sandbox experiments. *Water Resources Research* 47, no. 9: W09514. DOI:10.1029/2011WR010429.
- Bohling, G.C., J.J. Butler Jr., X. Zhan, and M.D. Knoll. 2007. A field assessment of the value of steady shape hydraulic tomography for characterization of aquifer heterogeneities. *Water Resources Research* 43, no. 5: W05430. DOI:10.1029/2006WR004932.
- Boulton, N.S. 1954. Unsteady radial flow to a pumped well allowing for delayed yield from storage. *International Association of Scientific Hydrology. Publication* 37: 472–477.
- Brauchler, R., R. Hu, L. Hu, S. Jiménez, P. Bayer, P. Dietrich, and T. Ptak. 2013. Rapid field application of hydraulic tomography for resolving aquifer heterogeneity in unconsolidated sediments. *Water Resources Research* 49, no. 4: 2013–2024. DOI:10.1002/wrcr.20181.
- Brauchler, R., R. Hu, P. Dietrich, and M. Sauter. 2011. A field assessment of high-resolution aquifer characterization based on hydraulic travel time and hydraulic attenuation tomography. *Water Resources Research* 47, no. 3: W03503. DOI:10.1029/2010wr09635.
- Brauchler, R., R. Hu, T. Vogt, D. Al-Halbouni, T. Heinrichs, T. Ptak, and M. Sauter. 2010. Cross-well slug interference tests: An effective characterization method for resolving aquifer heterogeneity. *Journal of Hydrology* 384, no. 1-2: 33–45. DOI:10.1016/j.jhydrol.2010.01.004.
- Butler, J.J. 2005. Chapter 2: Hydrogeological methods for estimation of spatial variations in hydraulic conductivity. In *Hydrogeophysics*. Water Science and Technology Library, Vol. 50, ed. Y. Rubin and S.S. Hubbard, 23–58. Dordrecht, The Netherlands: Springer.
- Cardiff, M., T. Bakhos, P.K. Kitanidis, and W. Barrash. 2013a. Aquifer heterogeneity characterization with oscillatory pumping: Sensitivity analysis and imaging potential. *Water Resources Research* 49, no. 11: 5395–5410. DOI:10.1002/wrcr.20356.
- Cardiff, M., W. Barrash, and P.K. Kitanidis. 2013b. Hydraulic conductivity imaging from 3D transient hydraulic tomography at several pumping/observation densities. *Water Resources Research* 49, no. 11: 7311–7326. DOI:10.1002/wrcr.20519.
- Cardiff, M., W. Barrash, and P.K. Kitanidis. 2012. A field proof-of-concept of aquifer imaging using 3D transient hydraulic tomography with modular, temporarily-emplaced equipment. *Water Resources Research* 48, no. 5: W05531. DOI:10.1029/2011WR011704.
- Cardiff, M., and W. Barrash. 2011. 3-D transient hydraulic tomography in unconfined aquifers with fast drainage response. *Water Resources Research* 47, no. 12: W12518. DOI:10.1029/2010WR010367.
- Castagna, M., and A. Bellin. 2009. A Bayesian approach for inversion of hydraulic tomographic data. *Water Resources Research* 45, no. 4: W04410. DOI:10.1029/2008WR007078.
- Chen, X., and J.F. Ayers. 1998. Aquifer properties determined from two analytical solutions. *Ground Water* 36, no. 5: 783–791.
- Ciabatti, P., and A. Pilia. 2004. Simulazione del flusso idrico sotterraneo dell'acquifero alluvionale multifalda della piana del Campidano meridionale (Sardegna). Quaderni di geologia applicata 1: Pitagora Editrice.
- Clemo, T. 2007. MODFLOW-2005 ground water model—User guide to the adjoint state based sensitivity process (ADJ). BSU CGISS Technical Report 07-01. Boise, Idaho: Boise State University.
- Cooper, H.H., and C.E. Jacob. 1946. A generalized graphical method for evaluating formation constants and summarizing wellfield history. *Eos, Transactions American Geophysical Union* 27, no. IV: 526–534.
- Einarson, M.D. 2006. Chapter 11: Multilevel ground-water monitoring. In *Practical Handbook of Environmental Site Characterization and Ground-Water Monitoring*, 2nd ed., ed. D. Neilsen, 808–848. Boca Raton, Florida: CRC Press.
- Einarson, M.D., and J.A. Cherry. 2002. A new multilevel ground water monitoring system using multichannel tubing. *Ground Water Monitoring & Remediation* 22, no. 4: 52–65.
- Gottlieb, J., and P. Dietrich. 1995. Identification of the permeability distribution in soil by hydraulic tomography. *Inverse Problems* 11, no. 2: 353–360.
- Harbaugh, A. 2005. MODFLOW-2005, the U.S. Geological Survey modular ground-water model—The ground-water flow process. U.S. Geological Survey Techniques and Methods 6-A16. Reston, Virginia: U.S. Geological Survey.
- Illman, W.A. 2014. Hydraulic tomography offers improved imaging of heterogeneity in fractured rocks. *Ground Water* 52, no. 5: 659–684.

- Illman, W., and P. Alvarez. 2009. Performance assessment of bioremediation and natural attenuation. *Critical Reviews in Environmental Science and Technology* 39, no. 4: 209–270. DOI:10.1080/10643380701413385.
- Jiménez, S., R. Brauchler, and P. Bayer. 2013. A new sequential procedure for hydraulic tomographic inversion. *Advances in Water Resources* 62, no. Part A: 59–70.
- Kitanidis, P.K. 1995. Quasi-linear geostatistical theory for inversing. *Water Resources Research* 31, no. 10: 2411–2419.
- Kitanidis, P.K., and E.G. Vomvoris. 1983. A geostatistical approach to the inverse problem in groundwater modeling (steady state) and one-dimensional simulations. *Water Resources Research* 19, no. 3: 677–690.
- Kramm, M.L., A.A. Keller, J. Rossabi, and L.G. Everett. 2001. DNAPL characterization methods and approaches, part 1: Performance comparisons. *Ground Water Monitoring & Remediation* 21, no. 4: 109–123.
- Lee, J., and P.K. Kitanidis. 2014. Large-scale hydraulic tomography and joint inversion of head and tracer data using the principal component geostatistical approach (PCGA). *Water Resources Research* 50, no. 7: 5410–5427. DOI:10.1002/2014WR015483.
- Leeson, A., and H. Stroo. 2011. SERDP and ESTCP workshop on investment strategies to optimize research and demonstration impacts in support of DoD restoration goals. SERDP ESTCP Workshop Report. 16 pp.
- Liu, S., T.-C.J. Yeh, and R. Gardner. 2002. Effectiveness of hydraulic tomography: Sandbox experiments. *Water Resources Research* 38, no. 4: 5-1–5-9. DOI:10.1029/2001WR000338.
- Liu, X., Q. Zhou, P.K. Kitanidis, and J.T. Birkholzer. 2014. Fast iterative implementation of large-scale nonlinear geostatistical inverse modeling. *Water Resources Research* 50, no. 1: 198–207. DOI:10.1002/2012WR013241.
- Liu, X., Q. Zhou, J. Birkholzer, and W.A. Illman. 2013. Geostatistical reduced-order models in underdetermined inverse problems. *Water Resources Research* 49, no. 10: 6587–6600. DOI:10.1002/wrcr.20489.
- Liu, X., and P.K. Kitanidis. 2011. Large-scale inverse modeling with an application in hydraulic tomography. *Water Resources Research* 47, no. 2: W02501. DOI:10.1029/2010WR009144.
- Liu, X., W.A. Illman, A.J. Craig, J. Zhou, and T.-C.J. Yeh. 2007. Laboratory sandbox validation of transient hydraulic tomography. *Water Resources Research* 43, no. 5: W05404. DOI:10.1029/2006WR005144.
- McElwee, C.D., and M.A. Yukler. 1978. Sensitivity of groundwater models with respect to variations in transmissivity and storage. *Water Resources Research* 14, no. 3: 451–459.
- Moench, A.F. 1994. Specific yield as determined by type-curve analysis of aquifer-test data. *Ground Water* 32, no. 6: 949–957.
- Neuman, S.P. 1975. Analysis of pumping test data from anisotropic unconfined aquifers considering delayed gravity response. *Water Resources Research* 11, no. 2: 329–342.
- Neuman, S.P. 1972. Theory of flow in unconfined aquifers considering delayed response to the water table. *Water Resources Research* 8, no. 4: 1031–1045.
- Nowak, W., and O.A. Cirpka. 2004. A modified Levenberg-Marquardt algorithm for quasi-linear geostatistical inversing. *Advances in Water Resources* 27, no. 7: 737–750.
- National Research Council (NRC). 2013. *Alternatives for Managing the Nation's Complex Contaminated Groundwater Sites*. Washington, DC: National Academies Press.
- National Research Council (NRC). 2005. *Contaminants in the Subsurface*. Washington, DC: National Academies Press.
- Pujol, J. 2007. The solution of nonlinear inverse problems and the Levenberg-Marquardt method. *Geophysics* 72, no. 4: W1–W16. DOI:10.1190/1.2732552.
- Sun, R., T.-C.J. Yeh, D. Mao, M. Jin, W. Lu, and Y. Hao. 2013. A temporal sampling strategy for hydraulic tomography analysis. *Water Resources Research* 49, no. 7: 3881–3896. DOI:10.1002/wrcr.20337.
- Vesselinov, V.V., S.P. Neuman, and W.A. Illman. 2001. Three-dimensional numerical inversion of pneumatic cross-hole tests in unsaturated fractured tuff 1: Methodology and borehole effects. *Water Resources Research* 37, no. 12: 3001–3017.
- Walton, W.C. 1970. *Groundwater Resource Evaluation*. New York: McGraw-Hill Book Co.